Organic light emitting devices with enhanced outcoupling via microlenses fabricated by imprint lithography

Yiru Sun
Princeton Institute for the Science and Technology of Materials (PRISM), Princeton University, Princeton, New Jersey 08544 and Department of Electrical Engineering, Princeton University, Princeton, New Jersey 08544

Stephen R. Forrest[a)]
Department of Electrical Engineering and Computer Science, University of Michigan, Ann Arbor, Michigan 48109; Department of Applied Physics, University of Michigan, Ann Arbor, Michigan 48109; and Department of Materials Science and Engineering, University of Michigan, Ann Arbor, Michigan 48109

(Received 9 May 2006; accepted 18 July 2006; published online 11 October 2006)

High efficiency white organic light emitting devices (WOLEDs) with optical outcoupling enhanced by hexagonal polymethylmethacrylate microlens arrays fabricated by imprint lithography on a glass substrate are demonstrated. Monte Carlo and finite difference time domain simulations of the emitted light are used to optimize the microlens design. The measured enhancement of light outcoupling and the angular dependence of the extracted light intensity are in agreement with the simulation. Using microlens arrays, we demonstrate a fluorescent/phosphorescent WOLED with a maximum external quantum efficiency of $(14.3\pm0.3)\%$ at 900 cd/m^2 and power efficiency of 21.6 ± 0.5 lm/W at 220 cd/m^2. The electroluminescent spectra at viewing angles from normal to the substrate plane, to 60° off normal, remain almost unchanged, giving a color rendering index of 87.
 [DOI: 10.1063/1.2356904]

I. INTRODUCTION

There has been considerable interest devoted to the optimization of white organic light emitting device (WOLED) efficiencies at high luminescence due to their potential use as interior illumination sources. For this purpose, it is essential to increase the outcoupling efficiency (η_{out}), i.e., the fraction of internally emitted photons that is extracted into the forward viewing space. Typically, $\eta_{out}\sim 20\%$ for OLEDs fabricated on planar glass substrates due to the difference between the refractive indices of air and the organic films comprising the device structure.[1] Hence, there is considerable potential for improvement in the external efficiency of OLEDs used for interior lighting as well as display applications. Indeed, enhancement of η_{out} also reduces the drive current density (J) needed to obtain a desired luminance, thereby leading to an increased WOLED operational lifetime.

Several methods of improving η_{out} have been reported, including the use of a resonant cavity,[2] excitation of surface plasmons,[3] insertion of a thin silica aerogel layer of very low refractive index,[4] and the use of periodic structures placed in the optically active layer to introduce Bragg scattering normal to the substrate plane.[5,6] However, these methods are often accompanied by undesirable attributes such as an angle dependent electroluminescent (EL) spectrum, angular variations in emission intensity, or complex and expensive fabrication processes. A method that avoids many of these shortcomings is the use of millimeter-sized lenses applied to the back side of the glass substrate.[7] However, large lenses must be aligned to each OLED, which is impractical for displays and is not useful for illumination sources where the OLED is typically several centimeters across.

An alternative is to use arrays of micron-scale lenses as introduced by Moller and Forrest.[8] In that work, an elastomeric polydimethylsiloxane (PDMS) sheet of a square array of microlenses was formed in a Si mold, and subsequently transferred to the surface of the glass substrate. This approach does not require alignment with the OLEDs, and due to their small diameter, η_{out} is largely independent of OLED size. One potential drawback of this method is that the soft lenses are subject to scratches and deformation occurring during lens preparation or usage. Here, we fabricate a hexagonal microlens array using polymethylmethacrylate (PMMA), whose Young's modulus is $E_{PMMA}=3.3$ GPa,[9] which is >1000 times that of PDMS.[10] The microlenses are directly integrated onto the glass substrate by imprint lithography. Using these arrays in conjunction with the recently introduced fluorescent/phosphorescent WOLED structure of Sun *et al.*,[11] we demonstrate WOLEDs with maximum external quantum and power efficiencies of $(14.3\pm0.3)\%$ at 900 cd/m^2, and 21.6 ± 0.5 lm/W at 220 cd/m^2, respectively. The average enhancement using microlens arrays versus a flat glass substrate is 1.49 ± 0.03. Light outcoupling is enhanced in the forward viewing half space without distorting or spectrally modifying the WOLED output.

II. SIMULATION OF MICROLENS PERFORMANCE

Typically, an OLED structure consists of a glass substrate coated with a transparent indium-tin-oxide (ITO) anode, followed by electrically and optically active organic

[a)]Electronic mail: stevefor@umich.edu

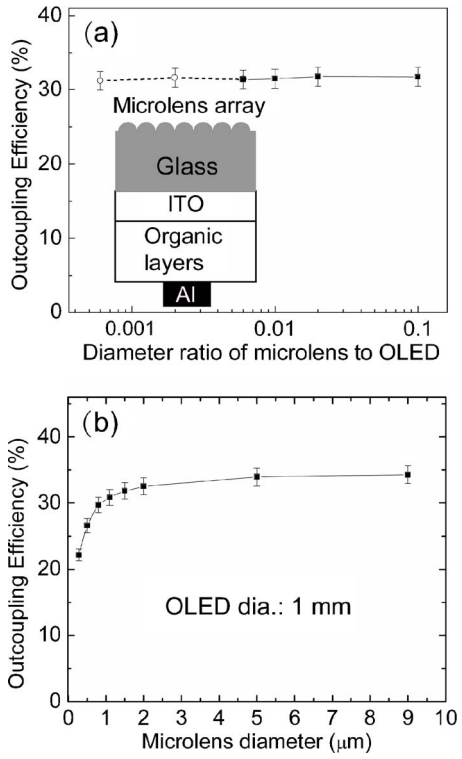

FIG. 1. (a) Outcoupling efficiency vs ratio of microlens to OLED diameter as calculated via 3D Monte Carlo simulations for hexagonal microlens arrays. Parameters used were refractive indices of the microlens and glass substrate of 1.45, and the corresponding microlens contact angle of the microlens shown in Fig. 2(a), inset, is $\theta=70°$. The open circles and dashed line indicate that ray optics may not be suitable when the microlens diameter approaches the light wavelength. Inset: Schematic of the OLED structure with the microlens arrays incorporated on the substrate; (b) outcoupling efficiency vs microlens diameter for an OLED with a 1 mm diameter, as calculated via wave optics finite difference time domain method, assuming emitting light wavelength is 550 nm. Note that the calculation differs from the ray optics solution in (a) as the microlens diameter approaches the light wavelength.

semiconductor layers, and capped by a metal cathode. For a flat glass substrate, the light escape cone is limited by the critical angle at the glass/air interface. By incorporating a microlens array onto the substrate surface opposite to the ITO [Fig. 1(a), inset] where the diameter of the individual microlens is significantly less than that of the OLED, the shaped substrate/air interface can redirect some of the high angle rays to lie within the escape cone, thereby increasing η_{out}. Furthermore, even when light is reflected from a lens into the substrate, it may be extracted after subsequent reflections from the metal cathode.

A hexagonal array of microlenses is used to provide a substrate coverage of 91%. To optimize the microlens design, we used three dimensional (3D) Monte Carlo simulations to trace a large number of rays generated at random positions, polarizations, and angles beneath the reflective, metallic WOLED cathode. At each material interface, the Fresnel equations are used to calculate the transmission and reflection coefficients. The refractive indices of the organics, ITO, glass, and air are $n_{org}=1.75$, $n_{ITO}=1.8$, $n_g=1.45$, and $n_0=1$, respectively.[1] For these calculations, we assume that the OLED diameter is always >10 times that of each microlens.

As expected from ray optics, when the shape and refractive index of the microlens are held constant, η_{out} is insensitive to diameter when it is much smaller than the OLED pixel diameter, but larger than the emitted light wavelength, as shown in Fig. 1(a). When the lens diameter is comparable to, or larger than the OLED itself, η_{out} depends on the relative position of the lens and the pixel. Simulations indicate that worst case misalignment of the OLED from the lens center (corresponding to the edge of the lens bisecting the OLED) can reduce η_{out} to $(11\pm2)\%$. On the other hand, when the microlens size approaches that of a wavelength, ray optics may not be an accurate means to calculate outcoupling efficiency.

Assuming a wavelength of $\lambda=550$ nm, light extraction from the substrate as a function of angle was simulated using a finite difference time domain model.[12] The total outcoupling fraction was then evaluated by integrating over the forward viewing half space with the weights decided by the angular light intensity distribution in the glass substrate, assuming isotropic emission from the organic films. Figure 1(b) shows that η_{out} for a 1 mm diameter OLED decreases rapidly as microlens diameter approaches λ. For diameters >5 μm, which is $\sim 10\lambda$, η_{out} converges to the result of the 3D Monte Carlo classical ray tracing simulation, with an asymptote of $\eta_{out}=(34\pm3)\%$.

The dependence of η_{out} on microlens refractive index (n_{ml}) for diameters >5 μm is shown in Fig. 2(a) (solid squares), suggesting that index matching to the substrate gives a maximum $\eta_{out}=(32\pm2)\%$. When the microlens index increases, the loss of photons due to total internal reflection at the microlens/air interface increases, although losses at the glass/microlens interface decreases. Compared to the simulated $\eta_{out}=(17\pm1)\%$ for a conventional flat glass substrate, the outcoupling is enhanced by a factor of $f\sim1.8$. In addition, for $n_{ml}=n_g$, Fig. 2(a) (open squares) shows that η_{out} increases as the microlens shape approaches that of a full 90° hemisphere. [The cone subtended by a microlens is described by the corresponding angle shown in Fig. 2(a), inset].

Enhanced light extraction is desired for both display and lighting applications, while displays also require a high image resolution. To quantitatively evaluate the extent of image blurring due to the lenses, we define an effective emission radius (R_e) where the light flux from the outcoupling surface drops to half of its maximum value at the center. For a conventional OLED with a 1-mm-thick flat glass substrate, R_e is calculated to be approximately 40% larger than the device radius ($R_{OLED}=0.5$ mm), as shown in Fig. 2(b). Using microlenses expands the escape cone and hence can cause image blurring. For the 1-mm-thick substrate with microlenses of radius $<0.1R_{OLED}$, simulations suggest that $R_e\approx2.1R_{OLED}$, resulting in a significant overlap of the emission areas of adjacent pixels. When the substrate thickness is reduced to 0.6 mm (typical of that used for commercial liquid crystal and OLED displays[13]), $R_e\approx1.4R_{OLED}$ which is comparable to a 1-mm-thick substrate without lenses. For even thinner substrates ($\leqslant100$ μm) with microlenses, $R_e\approx R_{OLED}$ according to simulations, i.e., the emissive aperture is almost the same as the device pixel size itself. A substrate thickness of ~100 nm is similar to the situation of a top emitting device

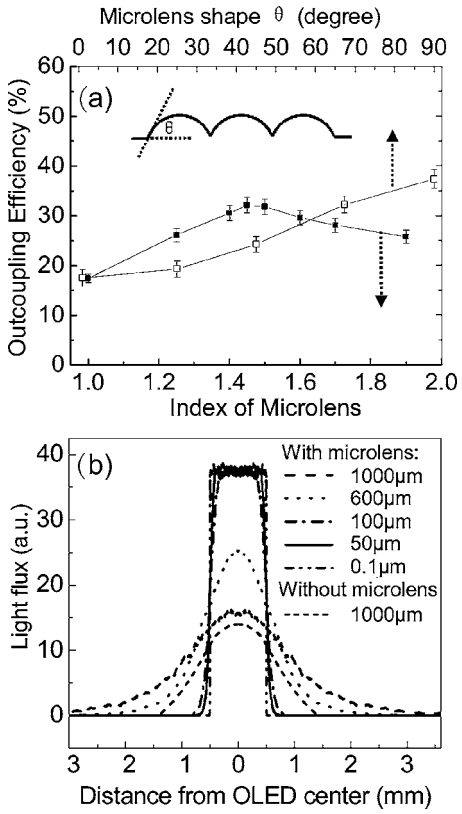

FIG. 2. (a) Outcoupling efficiency calculated as a function of microlens index of refraction (solid squares), assuming a $\theta=70°$ microlens shape; and as a function of the microlens shape (open squares) from flat ($\theta=0°$) to a full hemisphere ($\theta=90°$), assuming indices for the microlens and glass substrate are equal ($n_{ml}=n_g=1.45$). Inset: Definition of the contact angle of the cone with the substrate θ. (b) Simulated light flux on the outcoupling surface vs the distance from the OLED center as a function of glass substrate thickness, assuming an OLED radius of 0.5 mm.

with the microlenses applied directly onto the OLED surface. Since all the light is outcoupled within the device area, top emitting OLEDs are optimal for achieving high resolution and efficient display panels.[8]

III. EXPERIMENT

Based on the simulation results, we employed PMMA as the microlens material, whose index ($n_{PMMA}=1.48$) (Ref. 14) is very close to n_g. Microlenses with diameters of approximately 7 μm were incorporated on the glass substrate using imprinting technology by the process shown schematically in Fig. 3. For mold preparation, photoresist AZ-521415 (Ref. 15) was first spun on solvent-cleaned BK7 glass at 4000 rpm. Hexagonal arrays of 1.1-μm-diameter openings with 6.6 μm spacing distance were patterned on the photoresist following standard photolithographic methods. After a 10 min hard bake, the glass with patterned photoresist was soaked in buffered oxide etch (BOE, NH_4F 36 wt %:HF 4.6 wt %) diluted 10:1 with a surfactant for 6.7 min, and soaked in 1:1:5, $NH_4OH:H_2O_2:H_2O$ at 90 °C for 20 min to remove the photoresist. To ensure complete mold release after imprint lithography, the wet-etched glass was exposed to tridecafluoro-1,1,2,2-tetrahydrooctyltrichlorosilane in vacuum (~100 Torr) at 60 °C for 15 min to form a hydrophobic monolayer on the mold surface.[16]

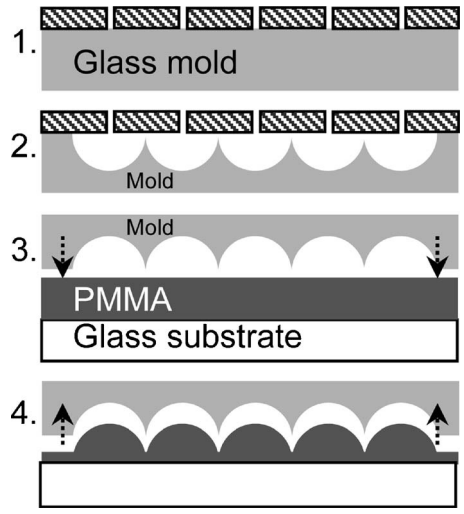

FIG. 3. Schematic of the mold preparation and imprint lithography process: hexagonal arrays of small openings are patterned on photoresist on a glass substrate (1). The substrate is wet etched in buffered oxide etch to achieve an approximately hemispherical shape (2). After the removal of the photoresist and the mold treatment, the mold is pressed against a thermal plastic PMMA layer on a second glass substrate at 200 °C (3) and released after cool down (4).

Prior to imprinting, a second glass substrate precoated with a 150-nm-thick, 20 Ω/sq ITO layer was first degreased in detergent solution and solvents. PMMA with M_w ~15 000 powder (10 g) was dissolved in 75 ml chlorobenzene at 80 °C. The solution was spun onto the glass substrate on the side opposite to the ITO coating at 1500 rpm. The substrate was then baked for 20 min at 90 °C to fully evaporate the chlorobenzene before placing the sample into a Nanonex NX2000 nanoimprinter.

A precleaned Si wafer was inserted between the ITO and a thermocouple to provide an accurate temperature reading as well as to protect the cleanliness of the ITO surface. The mold was placed on top of the glass substrate in contact with the PMMA layer. Prior to imprinting, the sample chamber was evacuated, followed by heating of both the mold and the sample to 200 °C, which is above the 105 °C glass transition temperature of PMMA.[17] A pressure of 240 psi was applied against the mold and sample for 4 min. The high pressure was maintained after the imprinting step until the temperature gradually dropped to below 45 °C.

The ITO surface of the substrate with microlenses, and a control sample with flat glass surface were both exposed to an UV/ozone flux at 20 mW/cm^2 for 5 min prior to loading into a vacuum system with a base pressure of 10^{-7} Torr. WOLEDs employing a fluorescent/phosphorescent doped emission layer[11] were simultaneously fabricated on both substrates. The device structure was 4-4′-bis[*N*-(1-naphthyl)-*N*-phenyl-amino]biphenyl (NPD) (33 nm)/5 wt % 4, 4′-bis(9-ethyl-3-carbazovinylene)-1,1′-biphenyl (BCzVBi) in 4,4′-N,N′-dicarbazole-biphenyl (CBP) (15 nm)/CBP (2 nm)/5 wt % iridium (III) bis (2-phenyl quinolyl-*N*,C$^{2'}$)acetylacetonate (PQIr) in CBP (6 nm)/6 wt % *fac*-tris(2-phenylpyridinato-*N*,C$^{2'}$) iridium(III) [Ir(ppy)$_3$] in CBP (12 nm)/CBP (1.5 nm)/5 wt % BCzVBi in CBP (10 nm)/4,7-diphenyl-1,10-phenanthroline (BPhen) (20 nm)/

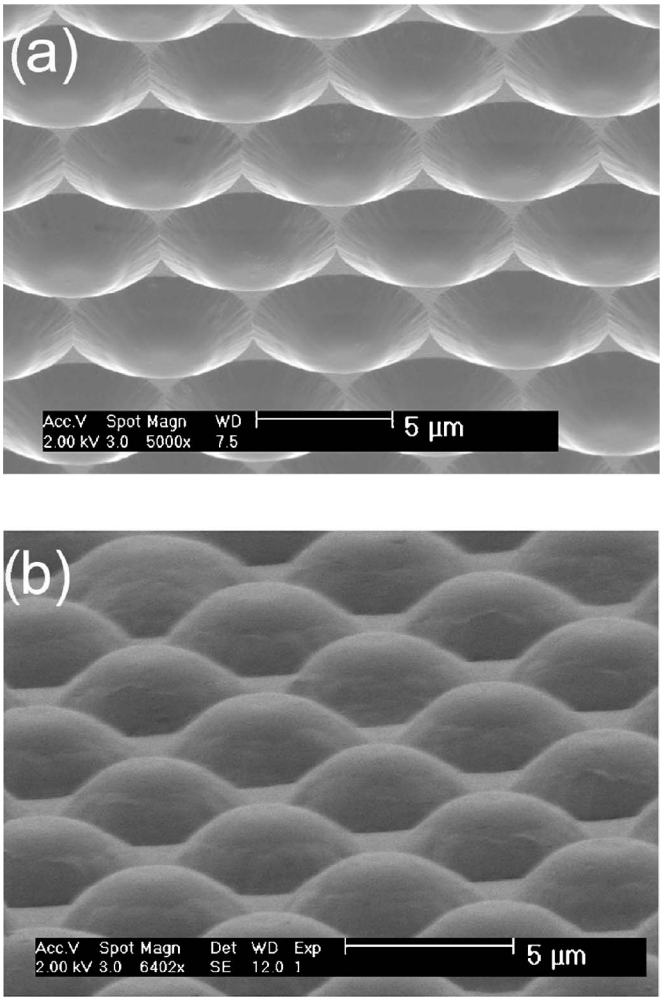

FIG. 4. (a) Scanning electron micrograph of the glass mold after wet etching and (b) of the imprinted microlens array.

BPhen mixed with Li in a 1:1 molar ratio (20 nm).[11] Finally, a cathode consisting of 8-Å-thick LiF followed by a 50-nm-thick Al layer was deposited through a shadow mask with an array of circular, 1.0-mm-diameter openings. Masking for cathode deposition was completed in a high purity nitrogen-filled glovebox with ~1 ppm water and oxygen. The WOLEDs were tested in the dark, using a calibrated Si photodiode with a 28×28 mm^2 detecting area,[18] and an HP 4156C semiconductor parameter analyzer following standard procedures.[19] The angular dependence of light emission was detected by a Si photodiode on a stage with azimuthal rotation.

IV. RESULTS AND DISCUSSIONS

Since glass is amorphous, wet etching in BOE with a small photoresist opening can result in an approximately hemispherical shape, thereby allowing for its use as a suitable mold for microlens imprinting [Fig. 4(a)]. Unlike the reflow method,[20] imprinting can avoid gaps between adjacent microlenses, providing a larger and adjustable microlens coverage on the substrate surface. Figure 4(b) shows a scanning electron micrograph (SEM) of the imprinted array consisting of 6.6 μm diameter $\times$2.2 μm high microlenses, corresponding to an OLED-to-lens diameter ratio of 150. The

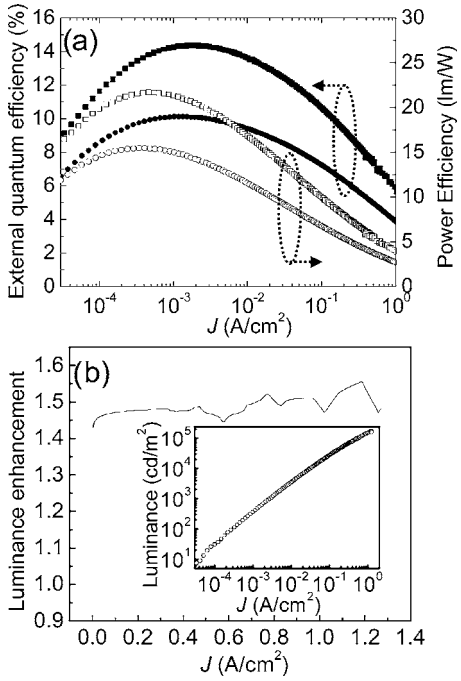

FIG. 5. (a) External quantum (solid) and power (open) efficiencies in the forward viewing space of WOLEDs on glass substrates with (squares) and without (circles) microlenses. (b) The enhancement of luminance of WOLEDs by using microlens arrays compared to a flat glass substrate as a function of current density. Inset: Luminance vs current density characteristics for WOLEDs with microlenses.

pattern on the mold was fully transferred into the PMMA layer on the substrate over a 2×2 cm^2 area, indicating that large scale fabrication is achievable. Indeed, by fabricating the mold on the surface of a cylinder, this method has potential for continuous, web-based imprinting over very large surfaces (e.g., 2×2 cm^2) such as are currently employed in the manufacture of liquid crystal displays.

The performance characteristics of the WOLEDs with microlenses are shown in Fig. 5(a) (squares). The maximum forward viewing external quantum and power efficiencies are $\eta_{ext}=(14.3\pm0.3)\%$ at 900 cd/m^2 and a current density of $J=2.4$ mA/cm^2, and $\eta_p=21.6\pm0.5$ lm/W at 220 cd/m^2 and $J=0.6$ mA/cm^2, respectively. At 5000 cd/m^2, η_{ext} and η_p fall slowly to 13.2% and 15.6 lm/W, respectively. For comparison, the performance of WOLEDs on flat glass substrates are also presented (circles), giving $\eta_{ext}=(10.1\pm0.3)\%$ and $\eta_p=14.2\pm0.3$ lm/W at 5000 cd/m^2, consistent with values reported previously for a similar structure.[11] The luminance versus current density characteristics of WOLEDs with microlenses are plotted in Fig. 5(b), inset. Figure 5(b) shows the enhancement of luminance versus J when using microlenses compared to a flat glass substrate. The average enhancement over the current density range of 0–1.2 A/cm^2 is $f=(1.49\pm0.03)$. Compared to the simulation in Fig. 2(a), this ratio corresponds to a 50° microlens, which is close to the microscopic measurement of $67°\pm10°$.

As a result of the improvement in η_{out} of 50%, the drive current density and energy consumption at a given luminance can be reduced by at least 33%, leading to potentially highly efficient lighting sources with significantly longer lifetimes. Moreover, a reduced current density leads to higher internal

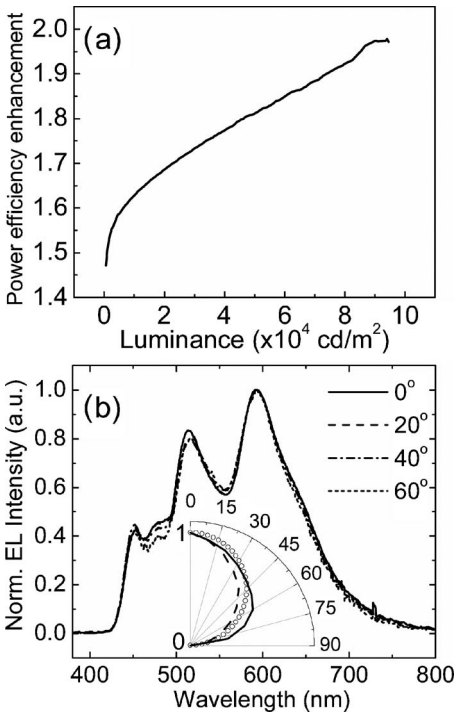

FIG. 6. (a) Enhancement of power efficiency of WOLEDs using microlens arrays compared to a flat glass substrate as a function of luminance. (b) Normalized electroluminescence spectra at a current density of $J=25$ mA/cm^2 as a function of viewing angle with respect to the substrate normal. Inset: Normalized light intensity vs viewing angle for WOLEDs on glass substrates with (solid line) and without (dashed line) microlenses; a Lambertian intensity output pattern (open circles) is also plotted for reference.

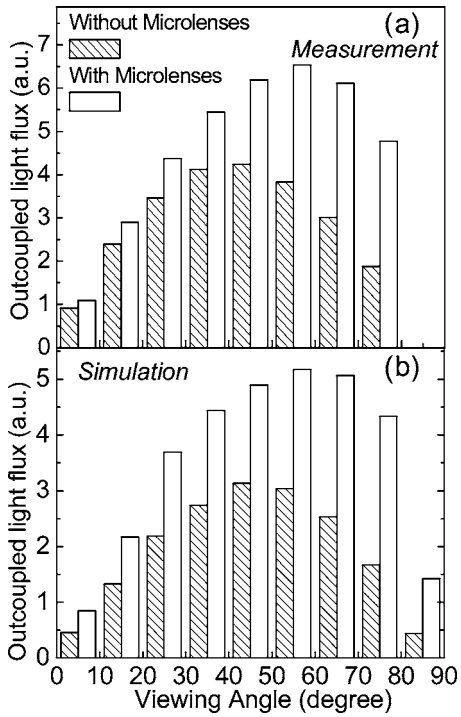

FIG. 7. (a) Outcoupled light flux vs viewing angle for both WOLEDs in Fig. 5 (b) Outcoupled light flux vs viewing angle for devices with and without microlens arrays as calculated via 3D Monte Carlo simulations.

efficiencies due to reduced rolloff at high J, such as triplet-triplet annihilation and exciton-polaron quenching. By interpolation of the control device power efficiency data from Fig. 5(a), we find that the efficiency can be up to 20% higher by operating the WOLED at 33% lower current density. This enhancement applies to both external and internal efficiencies, and can further reduce the energy consumption and drive current density at a desired luminance. Figure 6(a) plots the enhancement in power efficiency using microlens arrays versus a flat glass substrate as a function of luminance, showing the improvement is significant, especially at the highest luminance.

The electroluminescent spectra of the WOLEDs made on the glass substrate with microlenses measured at $J=25$ mA/cm^2 indicate a negligible dependence on viewing angle, from normal (0°) to 60° off normal to the substrate plane [Fig. 6(b)]. The spectra are also similar to those of the control WOLEDs. Correspondingly, the color rendering indices (CRIs) and Commission Internationale de L'Eclairage (CIE) coordinates are almost unchanged at various angles, from 87 and (0.396, 0.418) at 0° to 85 and (0.398, 0.423) at 60°, confirming that microlenses simply redirect the light without introducing microcavity or other parasitic optical effects.

Figure 6(b), inset, presents the normalized angular dependence of outcoupled light intensity of WOLEDs measured at $J=25$ mA/cm^2 for both the substrate with microlenses and the control sample in the forward viewing space. The latter is similar, but not identical to a Lambertian output pattern. The slight preference of the control WOLED for emission in the normal direction may account for the observation that the measured enhancement obtained with microlenses is not as large as the simulation predicts (Sec. II). From the angular intensity patterns, Fig. 7(a) illustrates the outcoupled light flux as a function of far field viewing angles for WOLEDs with and without microlenses, showing enhancement observed at all angles, especially at >50°. For comparison, Fig. 7(b) shows the outcoupled light flux versus viewing angle as simulated in Sec. II. The pattern and trend agree well with the measured data.

V. CONCLUSIONS

We used imprint lithography to fabricate close-packed hexagonal microlens arrays on the glass substrate of a fluorescent/phosphorescent WOLED, resulting in a maximum external quantum efficiency of $\eta_{ext}=(14.3\pm0.3)\%$ at 900 cd/m^2, and a maximum power efficiency of $\eta_p=21.6\pm0.5$ lm/W. The average outcoupling enhancement is $f=1.49\pm0.03$ compared to similar devices made on conventional, flat glass substrates. The emission spectra of WOLEDs on substrates with microlenses are largely independent of viewing angle, resulting in CRI=87, making this simple method for increasing light outcoupling attractive for lighting and displays. Models based on both ray and wave optics were used to simulate the microlens array performance, giving results consistent with the experimental data. In particular, microlenses placed on thin glass substrates or on the surfaces of top-emitting OLEDs can significantly improve light outcoupling while resulting in negligible degradation of high resolution display images.

ACKNOWLEDGMENTS

This work was partially supported by Department of Energy Solid State Lighting Program through a subcontract from the University of Southern California and Universal Display Corporation. The authors thank C. Peng, Q. Xia, and X. Liang at Princeton University for valuable discussions.

[1]V. Bulovic, V. B. Khalfin, G. Gu, P. E. Burrows, D. Z. Garbuzov, and S. R. Forrest, Phys. Rev. B **58**, 3730 (1998).
[2]T. Shiga, H. Fujikawa, and Y. Taga, J. Appl. Phys. **93**, 19 (2003).
[3]J. Feng, T. Okamoto, and S. Kawata, Appl. Phys. Lett. **87**, 2411109 (2005).
[4]T. Tsutsui, M. Yahiro, H. Yokogawa, and K. Kawano, Adv. Mater. (Weinheim, Ger.) **13**, 1149 (2001).
[5]J. M. Lupton, B. J. Matterson, I. D. W. Samuel, M. J. Jory, and W. L. Barnes, Appl. Phys. Lett. **77**, 3340 (2000).
[6]C. Hubert, C. Fiorini-Debuisschert, I. Hassiaoui, L. Rocha, P. Raimond, and J. M. Nunzi, Appl. Phys. Lett. **87**, 191105 (2005).
[7]M. H. Lu and J. C. Sturm, J. Appl. Phys. **91**, 595 (2002).
[8]S. Moller and S. R. Forrest, J. Appl. Phys. **91**, 3324 (2002).
[9]K. Yoshimoto, G. J. Papakonstantopoulos, J. F. Lutsko, and J. J. de Pablo, Phys. Rev. B **71**, 184108 (2005).
[10]A. Bietsch and B. Michel, J. Appl. Phys. **88**, 4310 (2000).
[11]Y. Sun, N. C. Giebink, H. Kanno, B. W. Ma, M. E. Thompson, and S. R. Forrest, Nature (London) **440**, 908 (2006).
[12]FULLWAVE, Version 1.0, RSoft, Inc., Ossining, NY, 2000.
[13]J. Bruinink, *Newsletter of the Society for Information Display Mid-Europe* (2000), Chap. 9, pp. 1–3.
[14]J. Brandrup and E. H. Immergut, *Polymer Handbook*, 3rd ed. (Wiley, New York, 1989).
[15]AZ Electronic Materials Corp., Somerville, NJ 08876.
[16]G. Y. Jung, Z. Y. Li, W. Wu, Y. Chen, D. L. Olynick, S. Y. Wang, W. M. Tong, and R. S. Williams, Langmuir **21**, 1158 (2005).
[17]S. Y. Chou, P. R. Krauss, and P. J. Renstrom, Science **272**, 85 (1996).
[18]Hamamatsu S3584-08, Hamamatsu City, Shizuoka Pref, 430–8587, Japan.
[19]S. R. Forrest, D. D. C. Bradley, and M. E. Thompson, Adv. Mater. (Weinheim, Ger.) **15**, 1043 (2003).
[20]M. K. Wei and I. L. Su, Opt. Express **12**, 5777 (2004).